HHS Public Access

Author manuscript

Mol Psychiatry. Author manuscript; available in PMC 2019 July 30.

Published in final edited form as:

Mol Psychiatry. 2020 October ; 25(10): 2504–2516. doi:10.1038/s41380-018-0325-9.

A kinome-wide RNAi screen identifies ERK2 as a druggable regulator of Shank3 stability

Li Wang[1,5], **Carolyn J. Adamski**[1,4,5], **Vitaliy V Bondar**[1,5], **Evelyn Craigen**[1,5], **John R. Collette**[2], **Kaifang Pang**[3,5], **Kihoon Han**[1,5,6], **Zhandong Liu**[3,5], **Richard N. Sifers**[2], **J. Lloyd Holder Jr.**[3,5,*], **Huda Y. Zoghbi**[1,3,4,5,*]

[1]Department of Molecular and Human Genetics, Baylor College of Medicine, Houston, TX 77030, USA

[2]Department of Pathology & Immunology, Baylor College of Medicine, Houston, TX 77030, USA

[3]Department of Pediatrics, Baylor College of Medicine, Houston, TX 77030, USA

[4]Howard Hughes Medical Institute, Baylor College of Medicine, Houston, TX 77030, USA

[5]Jan and Dan Duncan Neurological Research Institute at Texas Children's Hospital, Houston, TX 77030, USA

[6]Department of Neuroscience and Division of Brain Korea 21 Biomedical Science, Korea University College of Medicine, Seoul, 02841, South Korea

Abstract

Neurons are sensitive to changes in the dosage of many genes, especially those regulating synaptic functions. Haploinsufficiency of *SHANK3* causes Phelan-McDermid syndrome and autism, whereas duplication of the same gene leads to *SHANK3* duplication syndrome, a disorder characterized by neuropsychiatric phenotypes including hyperactivity and bipolar disorder as well as epilepsy. We recently demonstrated the functional modularity of Shank3, which suggests that normalizing levels of Shank3 itself might be more fruitful than correcting pathways that function downstream of it for treatment of disorders caused by alterations in *SHANK3* dosage. To identify upstream regulators of Shank3 abundance, we performed a kinome-wide siRNA screen and identified multiple kinases that potentially regulate Shank3 protein stability. Interestingly, we discovered that several kinases in the MEK/ERK2 pathway destabilize Shank3 and that genetic deletion and pharmacological inhibition of ERK2 increases Shank3 abundance *in vivo.* Mechanistically, we show that ERK2 binds Shank3 and phosphorylates it at three residues to promote its poly-ubiquitination-dependent degradation. Together, our findings uncover a druggable pathway as a potential therapeutic target for disorders with reduced *SHANK3* dosage, provide a rich resource for studying Shank3 regulation, and demonstrate the feasibility of this approach for identifying regulators of dosage-sensitive genes.

*Correspondence: holder@bcm.edu or hzoghbi@bcm.edu.

CONFLICT OF INTERESTS

The authors declare no conflict of interests.

INTRODUCTION

Alterations in protein levels that affect synaptic function can cause neuropsychiatric phenotypes such as autism spectrum disorder (ASD) and intellectual disability. One example of such a protein is SH3 and multiple ankyrin repeat domains 3 (Shank3). Deletion of one allele of *SHANK3* due to microdeletion of chromosome 22q13 causes Phelan-McDermid syndrome [1,2]. Point mutations and microdeletions within *SHANK3* are also associated with ASD [3,4]. Together, mutations in *SHANK3* account for about 1% of all ASD cases [4,5]. Moreover, we previously reported that duplication of *SHANK3* leads to increased activity, mood disorders, and epilepsy [6], indicating that a proper dosage of *SHANK3* is necessary for typical brain development. Furthermore, recent data have revealed epigenetic dysregulation of *SHANK3* in brain tissues from 15% of idiopathic ASD patients, suggesting that altered regulation and abundance of Shank3 might be a common cause of autism [7]. Currently, there are no targeted therapies for *SHANK3*-related disorders.

Current strategies for drug development in neuropsychiatric disorders largely focus on correcting a single dysregulated downstream pathway. However, in many neuropsychiatric disorders, including Phelan-McDermid syndrome, multiple downstream pathways are altered [8–11]. In our companion manuscript (Manuscript # 2018MP000080), we demonstrate the modularity of Shank3 function, which indicates that there is more than one independent pathogenic pathway downstream of Shank3 and correcting a single downstream pathway is unlikely to be sufficient for clear clinical improvement. An alternative strategy is to target the root of the disease: normalizing the abundance of Shank3 itself in individuals with haploinsufficiency or epigenetic dysregulation of *SHANK3*. Indeed, the reintroduction of *SHANK3* restores synaptic deficits in neurons derived from Phelan-McDermid syndrome patients [12]. Restoration of *Shank3* expression in adult *Shank3*-deficient mice rescues selective autism-like phenotypes [13]. However, treatment approaches for normalizing the level of Shank3 are lacking due to our limited understanding of its regulation.

Post-transcriptional repression of *SHANK3* by microRNAs including miR-7, miR-34a, and miR-504 has been reported [14], but these findings may have limited translational potential because microRNAs generally have broad effects and are difficult to target by small molecules. Other than that, there is a wealth of *SHANK3* regulatory circuitry to be discovered, particularly with respect to posttranslational modifications which often directly modulate a protein's stability. These regulations remain unknown largely because no one thus far has applied a comprehensive, unbiased approach to identify this type of regulation for Shank3. We, therefore, performed a genetic screen to identify regulators of Shank3 stability. We focused our screen on the human kinome because: 1) we found that Shank3 is extensively phosphorylated *in vivo* (see the companion manuscript), 2) phosphorylation is a common mechanism for regulating protein stability, 3) most importantly, kinases are readily targeted by small-molecule inhibitors. Our screen identified a novel regulatory mechanism that destabilizes Shank3 by phosphorylation-dependent ubiquitination/degradation. These findings provided a potential therapeutic target for Phelan-McDermid syndrome and a method for identifying therapeutic entry points for other neuropsychiatric disorders due to gene haploinsufficiency.

MATERIALS AND METHODS

Plasmids, antibodies, and primers

The information of plasmids, antibodies, and qRT-PCR primers used are listed in Supplementary Table 3.

Cell line culture and transfection

HEK293T (ATCC CRL-3216) and Daoy cells (ATCC HTB-186) were cultured in DMEM (Corning) containing 10% FBS (Atlanta Biologicals) and antibiotics (Penicillin/Streptomycin). HeLa cells (ATCC CCL-2) were cultured in MEM (Invitrogen) or DMEM (Corning) containing 10% FBS and antibiotics. Plasmids were transfected using TransIT-293 (Mirus), Lipofectamine 2000 (Invitrogen), or Lipofectamine 3000 (Invitrogen) and incubated for 30–72 hr, depending on downstream applications.

Virus generation

Viruses were generated as previously described with some modifications [15]. Briefly, lentiviral vectors (pHAGE, pGIPZ or pZIP) or MLV retroviral vector (pBABE-YFP-N-Shank3) and their respective packaging vectors (psPAX2 and pMD2G for lentivirus; pMD-MLVogp and pHDM-G for MLV retrovirus) were co-transfected into HEK293T cells in a 4:3:1 or 7:1:1 molar ratio respectively. Media was changed 24 hr following transfection to low volume media (5 mL for a 10 cm dish). Media was collected at 48 hr following transfection, replaced with fresh media (5 mL) and collected again at 72 hr. Viral supernatant was cleared from cell debris via filtration through a 0.45 μm polyethersulfone membrane (VWR). Cleared supernatants were concentrated using Lenti-X concentrator (Clontech) to 1/50 of the original volume. Viruses were titered by counting fluorescence-positive colonies.

Generation of stable cell lines

DsRed-IRES-EGFP, DsRed-IRES-EGFP-Shank3, and YFP-N-Shank3 cell lines were generated as previously described [15]. Briefly, for DsRed-IRES-EGFP and DsRed-IRES-EGFP-Shank3, each construct was cloned into a pHAGE vector (pLenti-GPS-GAW), packaged into lentiviruses and transduced into Daoy cells at very low multiplicity (less than 0.1) to favor single copy integration. Cells were selected by puromycin (1 mg/mL) and those double positive for DsRed and EGFP were sorted by fluorescence activated-cell sorting (FACS) into single cells. Single clones were expanded and one clone with low variation in EGFP/DsRed ratio was used for the screen. For YFP-N-Shank3 (N-terminal tagged) cell line generation, rat *Shank3* cDNA was cloned into pBABE-YFP-N (the first 155 N-terminal amino acids of YFP) vector, packaged into retroviruses and transduced into HeLa cells at low multiplicity (0.3). Cells were selected by G418 (0.5 mg/mL) before expansion and BiFC experiments.

Kinome-wide siRNA screen

The screen was performed as previously described [15,16]. Transgenic Daoy cells were plated onto 96-well round bottom plates. The following day, individual siRNAs were transfected by

0.08 μL Dharmafect (Dharmacon) at 20 nM final concentration and incubated for 72 hr before flow cytometry analysis. Flow cytometry was carried out on an LSRII Fortessa coupled with an HTS module (BD Biosciences). All siRNAs were tested in triplicates. Individual *t*-tests were performed on each siRNA by comparing them to the average of three scrambled siRNA sequences (with Low-, Medium-, and High-GC content) as controls for variability between triplicates. All the *p*-values were corrected for multiple hypothesis testing using false discovery rate control procedure [17]. All siRNAs with corrected *p*-values <0.05 were considered significant. A gene was considered a hit if at least two siRNAs tested against it significantly changed the ratio in the same direction and at least one of them changed the ratio more than 10%. Top 89 hits with robust changes in EGFP/DsRed ratio that are highly expressed in brain were subjected to secondary validation. The validation was performed by utilizing new siRNAs against the hits and tested in the same platform but including a DsRed-IRES-EGFP cell line as a negative control. Hits that significantly altered the EGFP/DsRed ratio in the DsRed-IRES-EGFP cell line more than 1/3 of that change in DsRed-IRES-EGFP-Shank3 cell line in the same direction were eliminated. See Supplementary Table 1 for detailed screen results.

Primary cortical neuron culture, drug treatment, virus infection, and western blot analysis

Mouse cortical neurons were prepared from E16.5 FVB/N mice and plated in poly-D-lysine coated 12-well plates (5×10^5 per well) in Neurobasal medium supplemented with GlutaMAX (Invitrogen), B-27, antibiotics (Penicillin/Streptomycin). Half of the media was changed with fresh media every 3–4 days. For drug treatment, DMSO (Sigma), pimasertib (2 μM, Selleckchem), or selumetinib (0.4 μM, Selleckchem) was applied to the media starting at days in vitro (DIV) 1. For shRNA virus infection experiments, neurons were infected with lentiviruses at DIV 1 with the multiplicity of infection at 10. Neurons were harvested at DIV 15–18 and lysed with RIPA buffer (50 mM Tris-HCl pH 8.0, 150 mM NaCl, 1 mM EDTA, 1 % NP-40, 0.5% sodium deoxycholate, 0.1% SDS) supplemented with phosphatase and protease inhibitors (GenDEPOT). Lysates were cleared by centrifugation (20 min, 15,000 rpm, 4°C) followed by protein quantification via BCA assay (Pierce). LDS Sample buffer (Invitrogen) with a reducing agent was added to each lysate followed by a 10 min incubation at 95°C. Samples were spun down and electrophoresed on a 4–12% Bis-Tris gel, transferred to a nitrocellulose membrane and blocked for one hour with 5% non-fat milk prior to primary antibody incubation. Unless otherwise indicated, the samples used for western blot were from whole lysates.

RNA extraction and quantitative real-time PCR (qRT-PCR)

RNA extraction and qRT-PCR were performed as previously described [18]. Briefly, total RNA was purified using the miRNeasy kit (Qiagen) according to the manufacturer's instructions. RNA quantity and quality was checked using NanoDrop 1000 (Thermo Fisher). cDNA was synthesized by Quantitect Reverse Transcription kit (Qiagen). qRT-PCR was performed using the CFX96 Touch Real-Time PCR Detection System (Bio-Rad) with iTaq Universal SYBR Green Supermix (Bio-Rad). Real-time PCR results were analyzed using the comparative Ct method normalized against the housekeeping gene *Gapdh*. Primers used were listed in Supplementary Table 3.

Animals

Mice were housed in an AALAS-certified Level 3 facility on a 12-hour light cycle. The following available mouse lines were used: B6.Cg-Tg(Nes-cre)1Kln/J (Jackson Laboratory JAX003771), B6.129-Mapk1^{tm1Gela}/J (Jackson Laboratory JAX019112), B6.129-*Shank3*^{tm2Gfng}/J (Jackson Laboratory JAX017688), and FVB-Tg (Shank3-EGFP)1Hzo/J (In-house, but mice with the same allele on the C57BL6/J background are available at Jackson Laboratory JAX024033). *Erk2* nestin-cre conditional knockout mice were generated by crossing *Erk2*$^{flox/+}$ mice with Nestin-cre; *Erk2*$^{flox/+}$ mice. *Shank3B*$^{+/-}$ mice were generated by crossing *Shank3B*$^{+/-}$ to *Shank3B*$^{+/-}$ mice. Both male and female mice were used for the biochemical analysis. All procedures to maintain and use these mice were approved by the Institutional Animal Care and Use Committee for Baylor College of Medicine.

Crude synaptosomal fractionation

P2 (crude synaptosomal fraction) subcellular fractions were prepared as described [19].

Drug injection in mice

Treatment with the PD0325901 compound (Selleck) was performed on WT or *Shank3B*$^{+/-}$ mice on the C57BL6/J background. The compound was solubilized in 5% NMP, 5% solutol, HS-15, 90% saline with a final concentration of 1 mg/ml. The carrier solution (for the control group) and the solubilized drug (for the treatment group) were aliquoted and stored at −80°C. All experimenters were blinded to the drugs. Aliquots were thawed in a 37°C bath prior to the AM injection and disposed of at the end of the day. Mice in the treatment group received 5mg/kg drug BID 6 days per week. Injection volumes ranged from 70 to 140 microliters and were adjusted on a weekly basis according to individual weights. After 4 weeks of treatment, the cortex was harvested within 4 hours of the last injection and snap frozen in liquid nitrogen. For experiments in which only the whole lysate was needed, samples were homogenized in 50 mM Tris pH 7.5, 0.5% NP-40, 150 mM NaCl, 1 mM EDTA supplemented with protease and phosphatase inhibitors (GenDEPOT). For experiments in which both the whole lysate and the P2 fraction were needed, samples were prepared as described [19], then the whole homogenate was solubilized by adding NP-40 to 0.5% final concentration. Lysates were then normalized based on total protein levels and prepared in LDS sample buffer supplemented with reducing sample buffer (Invitrogen).

Quantification of Shank3 and individual isoforms in western blot

The number of Shank3 isoforms is not entirely clear. However, several major isoforms of Shank3 have been reported [20]. The antibody we used to blot Shank3 is the H-160 antibody from Santa Cruz, which is raised against the amino acids 1431–1590 in C-terminal of human Shank3. We defined three strong bands of Shank3 between 150 kD and 190 kD as the three major isoforms of Shank3 (referred to as Shank3α [top two overlapping strong bands], Shank3β [a moderately strong band in the middle], and Shank3γ [a strong band at bottom] based on molecular weight [high to low]). These three major isoforms correspond to Shank3a, Shank3c/d, and Shank3e as described previously [20]. Densitometry analysis was done using ImageJ's Analysis/Gel/Plot Lanes function. For each isoform, the area under a

curve value is separately detected and used as the isoform abundance value. For total Shank3, the values of the area under a curve of all the isoforms were combined and used as the total Shank3 abundance value.

Immunoprecipitation of EGFP-Shank3 from *EGFP-Shank3* transgenic mice

The whole procedure was essentially the same as described [6] except that only striatal tissue was used here. Briefly, Striata were dissected from 4 animals (11-week-old) per each genotype (wild-type and *EGFP-Shank3* transgenic mice), and crude synaptosomal fraction solubilized with DOC buffer was prepared. The solubilized synaptosomal fraction was dialyzed against dialysis buffer (50 mM Tris-HCl, pH 7.4, 0.1% TritonX-100) overnight. Then, 1mg of lysates were incubated with GFP-Trap beads (ChromoTek) for 2 hr at 4 °C. The beads were briefly washed dialysis buffer, boiled with NuPAGE LDS sample buffer (Invitrogen) with a reducing agent, and subjected to western blot analysis.

Bimolecular fluorescence complementation (BiFC) assay

BiFC assay was performed as previously described with modifications [21]. Briefly, HeLa cells stably express YFP-N-Shank3 (‘Bait’) were transfected with 500 ng ‘Prey’ plasmid (expressing ERK2, MSK1, PKAα, cortactin, homer containing the C-terminal portion of YFP [amino acid 156–239]). Cells were cultured for another 72 hr and collected for flow cytometry analysis using a BD LSRII Fortessa to quantify the percentage of YFP positive cells.

Shank3 fragments purification

Complementary DNAs of ten Shank3 fragments were cloned into a pDEST15 vector (GST-tagged, Invitrogen) and then transformed into BL21AI (Invitrogen). GST-Shank3 fragments were purified by glutathione sepharose 4B (GE) precipitation, eluted by 10 mM glutathione, and dialyzed against dialysis buffer (50 mM Tris-HCl pH 7.4, 150 mM NaCl, 0.25 mM dithiothreitol [DTT], 10% glycerol). 1 μg of each purified fragment was run on a 4–12% Bis-Tris gel and visualized by Coomassie Brilliant Blue stain (Bio-Rad) according to manufacturer’s instructions.

In vitro kinase assay for mass spectrometry

1 μg Shank3 fragment and 0.3 μg of active kinase (ERK2 [Sigma], PKAα [Millipore], GSKβ [SignalChem] or CK2α [SignalChem]) were mixed in 15 μl kinase reaction buffer (40 mM Tris-HCl pH 7.5, 20 mM $MgCl_2$, 0.1 mg/mL BSA, 2 mM DTT and 100 μM ATP [Promega]) and incubated at 30 °C for 2 hr. The kinase reactions were terminated by addition of NuPAGE LDS sample buffer and sample reducing agent (Invitrogen) and boiled for 15 min. The boiled samples were subjected to mass spectrometry analysis.

LC-MS/MS Analysis and data validation

Samples were subjected to SDS-PAGE (NuPAGE 10% Bis-Tris Gel, Invitrogen). Proteins were visualized with Coomassie Brilliant Blue stain and the target proteins with expected molecular weights were excised from the gel according to molecular size. The individual gel piece was destained and subject to in-gel digestion using trypsin (GenDepot T9600). The

tryptic peptides were resuspended in 10 μL of loading solution (5% methanol containing 0.1% formic acid) and subjected to nanoflow LC-MS/MS analysis with a nano-LC 1000 system (Thermo Scientific) coupled to Orbitrap Elite (Thermo Scientific) mass spectrometer. The peptides were loaded onto a Reprosil-Pur Basic C18 (1.9 μm, Dr. Maisch GmbH, Germany) precolumn of 2 cm×100 μm size. The precolumn was switched in-line with an in-house 50 mm×150 um analytical column packed with Reprosil-Pur Basic C18 equilibrated in 0.1% formic acid/water. The peptides were eluted using a 35min discontinuous gradient of 4–26% acetonitrile/0.1% formic acid at a flow rate of 800 nL/min. The eluted peptides were directly electro-sprayed into Orbitrap Elite mass spectrometer operated in the data-dependent acquisition mode acquiring fragmentation spectra of the top 25 strongest ions and under the direct control of Xcalibur software (Thermo Scientific). Obtained MS/MS spectra were searched against the target-decoy mouse RefSeq database in Proteome Discoverer 1.4 interface (Thermo Fisher) with Mascot algorithm (Mascot 2.4, Matrix Science). The precursor mass tolerance was confined within 20 ppm with fragment mass tolerance of 0.5 Daltons and a maximum of two missed cleavage allowed. Dynamic modifications of Oxidation, protein N-terminal Acetylation, Destreak and Phosphorylation on serine, threonine, and tyrosine were allowed. The peptides identified from mascot result file were validated with 5% false discovery rate (FDR) and subject to manual verifications for correct assignment.

LC-MS/MS Peptide quantification

The PD1.4 result file and the .RAW file from MS were then imported to Skyline software [22] in order to carry out relative quantification. Each individual peptide was validated by checking for its ID from the PD1.4 result and the missing peptides were selected by the match-by-run approach. The area under a curve (AUC) for each peak was adjusted based on the retention time. Finally, the sum of AUC of top 3 strongest productions per each precursor ion (for each peptide) was calculated.

Pulse-chase protein stability assay

HeLa cells cultured in 6-well plates were transfected with 500 ng plasmids expressing HA-Shank3 (WT or 3A) by Lipofectamine 3000. 30 hr later, methionine starvation was performed for 1hr by changing the culture media with 1 mL pulse medium (DMEM high glucose without L-glutamine, sodium pyruvate, L-methionine, and L-cysteine [Gibco] + 10% FBS + 2 mM L-glutamine) into each well. After methionine starvation, pulse medium was changed by labeled pulse medium (pulse medium plus 100 μCi ^{35}S methionine/cysteine [PerkinElmer]) and cells were incubated for 30min. After labeling, cells were washed with warm PBS for 3 times and then 1 mL chase medium (DMEM + 10% FBS + 2mM L-methionine) was added into each well. Cells were harvested at indicated time points after adding chase medium. Harvested cells were lysed in 1 mL DOC buffer (50 mM Tris-HCl pH 9.0, 5mM EDTA, 1% sodium deoxycholate) supplemented with phosphatase and protease inhibitors (GenDEPOT) and incubated with anti-HA-agarose beads (Sigma) for 2 hr at 4 °C. The beads were washed with DOC buffer for 3 times, boiled with NuPAGE LDS sample buffer (Invitrogen) to elute proteins. The eluted products were run on an SDS-PAGE gel. The gel was fixed for 30 min in a 2% salicylic acid, 30% methanol solution and dried before detection by autoradiography.

Ubiquitination assay

HEK293T cells were cultured in 6-well plates and transfected with 500 ng pCI-His-hUbi and 500 ng empty vector or vectors expressing Shank3 variants (WT or 3A). 30 hr after transfection, cells were treated with 20 μM MG-132 (Millipore) for 8 hr, and then harvested in RIPA buffer supplemented with MG-132 (20 μM), N-ethylmaleimide (20 mM), and protease/phosphatase inhibitors. The lysates were incubated with anti-HA-agarose beads (Sigma) for 2 hr at 4 °C. After incubation, the beads were washed in lysis buffer. Proteins were eluted by boiling the beads with NuPAGE LDS sample buffer and subjected to western blot analysis.

Statistical analysis

All data in figures were presented as mean ± s.e.m. (standard error of the mean). All comparisons were two-sided. All statistical details and statistical significance were indicated in the figure legends. Normality was determined using the D'Agostino and Pearson omnibus normality test and Shapiro-Wilk normality test. *p<0.05, **p<0.01, ***p<0.001, ****p<0.0001, NS, not significant.

RESULTS

A kinome-wide RNAi screen to identify posttranslational regulators of Shank3 stability

To identify potential posttranslational regulators of Shank3 stability, we engineered a Daoy cell line (human medulloblastoma-derived cell) to express a transgene controlled by a CMV promoter. The transgene is composed of the cDNA encoding DsRed, an internal ribosomal entry site (IRES), and the cDNA encoding N-terminal EGFP-tagged rat Shank3. In these transgenic cells, DsRed and EGFP-Shank3 were independently translated from the same transcript (Figure 1a). This bicistronic reporter system allowed us to monitor the steady-state Shank3 level normalized to transgene expression by accessing the EGFP-to-DsRed fluorescence ratio through flow cytometry. This system has been successfully used in other fields such as cancer, neurodegeneration, and more recently in MeCP2 regulation [15,16,23–25].

Using this reporter system, we tested the effect of each of the 1,908 siRNAs targeting all 636 known kinase or kinase-like genes (3 siRNAs per gene) on Shank3 stability using flow cytometry (Figure 1b,c and Supplementary Table 1). We considered a gene as a hit if it met two criteria: two or more siRNAs targeting it significantly (adjusted p-value < 0.05) altered the EGFP-to-DsRed ratio in the same direction, and at least one of these siRNAs changed the ratio more than 10%. Applying these criteria resulted in 134 hits that, when targeted by siRNAs, increased the ratio (destabilizers of Shank3) and 75 that decreased it (stabilizers of Shank3) (Supplementary Table 1).

One limitation of our reporter system is that it can identify kinases that impact EGFP stability, DsRed stability, or IRES efficiency as false positive hits. To eliminate these, we selected 89 hits (59 destabilizers and 30 stabilizers) from the primary screen based on their expression level in neurons as well as robustness in ratio change and performed a secondary screen on them. In this secondary screen, we compared the effect of an siRNA in the screen cell line with that in a control cell line (DsRed-IRES-EGFP). Those siRNAs that caused a

similar ratio change in the control cell line were eliminated. This secondary screen validated 39 kinases as posttranslational regulators of Shank3 stability (Figure 1d and Supplementary Table 1). Interestingly, we found that many hits which, when targeted by siRNAs, increased Shank3 stability (destabilizers of Shank3) belong to the canonical Mitogen-activated protein kinase kinase (MEK)/ Extracellular signal-regulated kinase (ERK) signaling pathway (Figure 1d-f). We, therefore, decided to focus on this pathway for further validation.

Inhibition of MEK/ERK pathway increases Shank3 abundance

To test whether the MEK/ERK pathway regulates Shank3 abundance in neurons, we cultured mouse primary cortical neurons and treated them with two different highly selective MEK inhibitors pimasertib and selumetinib. Both inhibitors efficiently inhibited MEK activity as indicated by a profound reduction of phospho-ERK1/2 (Figure 2a,c). Both inhibitors increased Shank3 protein abundance (Figure 2a-d). Note that the mRNA levels of Shank3 are not affected by these inhibitors, indicating a posttranscriptional regulation (Supplementary Figure 1a,b).

In the canonical MEK/ERK pathway, there are two ERK kinases downstream of MEK: ERK1 and ERK2. To determine which ERK regulates Shank3 abundance, we used shRNA to deplete each of them in primary cortical neurons. Both shRNAs significantly reduced their target proteins (Figure 2e-g). While depleting *Erk1* had no effect on Shank3 abundance, depleting *Erk2* increased Shank3 abundance, indicating that ERK2 is the primary kinase responsible for Shank3 regulation in this pathway (Figure 2e,h).

To validate our findings *in vivo*, we chose two independent methods: pharmacological inhibition and genetic knockout (KO). For pharmacological inhibition, we used PD0325901, a selective, highly potent MEK inhibitor with a long half-life *in vivo* [26]. Systematic treatment with PD0325901 for four weeks not only inhibited MEK/ERK signaling but also increased Shank3 abundance in the cortex of mice (Figure 3a-c). For genetic KO, we generated *nestin-cre*; *Erk2*$^{flox/flox}$ conditional KO (cKO) mice to specifically delete *Erk2* in the brain (*Erk2* whole-body KO mice are embryonic-lethal). We found that deletion of *Erk2* in the brain did not increase Shank3 in the whole cortical lysate, potentially due to a partial developmental compensation (Supplementary Figure 2a,b). Interestingly, we found that deletion of *Erk2* increased Shank3 abundance in the crude synaptosomal fraction (P2) of the cortex (Figure 3d,e). It is possible that the higher concentration of Shank3 in the synaptosomes renders Shank3 more responsive to the manipulation of ERK2 activity. Consistent with this, PD0325901 injection failed to increase Shank3 in the whole cortical lysate of *Shank3B* heterozygous mice, in which the baseline abundance of Shank3 is halved (Supplementary Figure 2c-e). However, the same treatment still increased Shank3 abundance in the P2 fraction from *Shank3B* heterozygous mice (Figure 3f-h). Together, these results demonstrate that reducing the ERK2 activity or levels increases Shank3 abundance *in vivo*, and this regulation is more prominent in synaptosomes compared with other cellular compartments.

ERK2 phosphorylates Shank3 to promote its ubiquitination and degradation

Next, we investigated how inhibiting ERK2 increases Shank3 abundance. We reported that Shank3 is phosphorylated at multiple residues in our companion manuscript. It is possible that ERK2 interacts and phosphorylates Shank3 to regulate its stability. Immunoprecipitation of Shank3 from the striatum of *EGFP-Shank3* transgenic mice demonstrated that Shank3 and ERK2 formed a protein complex *in vivo* (Figure 4a). To determine whether this interaction is direct or not, we performed a bimolecular fluorescence complementation assay [21]. In this assay, the direct interaction between Shank3 and the tested protein will bring two complimentary YFP fragments YFP-N and YFP-C (tagged to Shank3 and the tested protein, respectively) within proximity resulting in a conformational change to a functional, stable YFP that can be detected by flow cytometry (Figure 4b). We engineered a cell line to express YFP-N-Shank3, then transfected these cells with vectors that express a panel of YFP-C-tagged proteins. We found that, like other well-established Shank3 interactors (Protein kinase A alpha catalytic subunit [PKAα], cortactin, and Homer), YFP-C-tagged ERK2 transfection could elicit a strong fluorescent signal, while a nucleus-enriched kinase MSK1 could not (Figure 4c). These results demonstrate that ERK2 directly interacts with Shank3.

To determine whether ERK2 phosphorylates Shank3 directly, we performed an *in vitro* kinase assay. Because its large size makes full-length Shank3 difficult to purify from bacteria, we purified ten fragments of Shank3 covering the entire protein and used each fragment in an *in vitro* kinase assay (Figure 4d). We found, in total, eighteen residues were phosphorylated by ERK2 *in vitro* (Supplementary Table 2). Thus, it is possible that ERK2 regulates Shank3 abundance through phosphorylating multiple residues critical for its stability. To prioritize which residues are critical, we applied two criteria. First, we required the residue to be phosphorylated *in vivo*. Second, since we consistently observed a trend of increase in all the three major isoforms of Shank3 upon inhibition/depletion of ERK2 (Supplementary Figure 3a-n), we required the residue to be present in all the three major isoforms. Three residues met these criteria: S1134, S1163, and S1253 (Figure 4e-g). We also performed an *in vitro* kinase assay with Protein kinase A alpha catalytic subunit (PKAα), Glycogen synthase kinase 3 beta (GSK3β), and Casein kinase 2 (CK2) which all interact with Shank3 (data not shown) to evaluate specificity. Except for S1134 which was also phosphorylated by CK2, none of the three sites were phosphorylated by other kinases (Supplementary Table 2).

To determine the impact of pS1134, pS1163, and pS1253 on Shank3 stability, we performed site-directed mutagenesis to generate a vector expressing a mutant Shank3 in which all the three serines were substituted by alanine to abolish phosphorylation (referred to as 3A Shank3). We then transfected vectors either expressing wild-type (WT) Shank3 or 3A Shank3 in HeLa cells. The stability of newly-synthesized Shank3 proteins was analyzed by ^{35}S-methionine/cysteine pulse-chase radiolabeling. We determined that the 3A Shank3 had decreased protein turnover relative to WT Shank3 (Figure 5a,b), suggesting that phosphorylation events at these three serines promote Shank3 degradation.

The abundance of Shank family proteins can be regulated by ubiquitination-dependent degradation [27]. It is conceivable that phosphorylation destabilizes Shank3 by promoting its

poly-ubiquitination. We, therefore, performed a ubiquitination assay to test this. We co-expressed ubiquitin and Shank3 in cultured cells then immunoprecipitated Shank3 to quantify its degree of ubiquitination. We found that 3A Shank3 exhibited decreased ubiquitination relative to WT Shank3 (Figure 5c,d), consistent with a model that ERK2 phosphorylates Shank3 and destabilizes it by promoting its ubiquitination (Figure 5e).

DISCUSSION

Normalizing Shank3 abundance could be beneficial for genetic disorders caused by alterations in *SHANK3* dosage. Here, through a kinome-wide RNAi screen, we identified the MEK/ERK2 pathway as a regulator of Shank3 stability. Reducing ERK2 kinase activity increased Shank3 abundance *in vivo*. We also determined that phosphorylation of Shank3 by ERK2 at selective residues promotes its ubiquitination and degradation.

The involvement of kinases in the modulation of Shank3 function, both upstream and downstream, has long been recognized. RSK2 is the first kinase reported that phosphorylates Shank3 to regulate synaptic transmission [28]. CLK2 and Akt kinase signaling are downstream pathways dysregulated upon loss of Shank3, and modulation of CLK2 corrects several phenotypes in *Shank3*-deficient neurons [9]. In this study, we further expanded our understanding of the kinase-dependent Shank3 regulation through a comprehensive, unbiased screen that focused on protein stability. The screen presented above highlights two important aspects of biology that have clinical implications: the regulatory mechanisms of Shank3 and putative insights into related neurodevelopmental disorders. On the one hand, understanding the regulatory mechanisms of Shank3 could help us identify potential therapeutic targets—including MEK and ERK2—for individuals with *SHANK3* haploinsufficiency. On the other hand, knowing that reduced Shank3 level causes intellectual disability (ID) and ASD, the regulators we identified from the screen that normally act to stabilize Shank3 could be potential risk factors for neurodevelopmental disorders themselves. This is because deleterious mutations in those genes potentially could lead to reduced Shank3 abundance in patients harboring those mutations which may contribute to their phenotypes. Supporting this notion, mutations in stabilizers *TAF1*, *TRIO* and *SIK1* have been found in individuals with ID and/or ASD (Supplementary Table 1) [29–31].

Though we found MEK/ERK2 pathway as a potential therapeutic entry point for *SHANK3* haploinsufficiency, it is important to note that targeting this pathway alone is not likely to be enough to fully normalize Shank3 abundance or related phenotypes. First of all, the effect size of ERK2 inhibition on Shank3 is between 20% and 40% depending on the experimental setting. In some conditions, the increase of Shank3 was only observed in the synaptic fraction, but not in the whole tissue lysate. Additionally, MEK/ERK2 pathway is a master signaling pathway, regulating a number of cellular events. Chronic inhibition ERK2 may not be a selective therapy for autism, potentially causing undesired side effects [32]. Thus, it is necessary to identify/validate additional regulators for potential combinational therapy.

Previous studies reported that the abundance of Shank family proteins is dynamically regulated within the PSD via the ubiquitin-proteasome system [27]. Additionally, neuronal activity can alter Shank3 protein stability and abundance through changes in GKAPs [33].

However, detailed mechanisms underlying Shank3 ubiquitination and degradation are largely unknown. To our knowledge, ERK2 is the first kinase identified that directly phosphorylates Shank3 to promote its degradation. Future studies could provide more insight to determine whether the neuronal activity or GKAPs regulate Shank3 through ERK2. In addition, the 3A Shank3 mutant is still ubiquitinated, even if to a lesser extent, suggesting the existence of independent signaling pathways that regulate Shank3 ubiquitination. It is also worth noting that both the kinase assays and the ubiquitination assays were conducted using either recombinant proteins or heterologous expression systems but not *in vivo* due to technical difficulties. The *in vivo* relevance of the proposed mechanism will require further investigation.

Overexpression of *SHANK3* via chromosomal duplication also causes a neuropsychiatric disorder [6]. In our screen, we have also identified candidate genes that when inhibited decrease Shank3 abundance. These candidate genes could be valuable targets for *SHANK3* duplication patients. Together, we believe our genetic screen not only elucidated an important post-translational regulatory mechanism of Shank3 but also demonstrated the feasibility of this approach for identifying regulators of dose-sensitive genes for potential therapeutic entry points.

Supplementary Material

Refer to Web version on PubMed Central for supplementary material.

ACKNOWLEDGMENTS

We are grateful to Antrix Jain and Sung Y. Jung for their help in mass spectrometry; Zhou Songyang, Dan Liu, and Jun Xu for providing plasmids and help for the BiFC assay; Maxime WC Rousseaux, Nan Lu, Laura Lombardi, Paymaan Jafar-Nejad, Jeehye Park, and all Zoghbi lab members for technical assistance and insightful discussions on this work. This work was supported by the Howard Hughes Medical Institute (H.Y.Z.), a gift from Mr. Charif Souki (to the Jan and Dan Duncan Neurological Research Institute), Autism Speaks (grant #9120 to L.W.), NINDS K08 Award NS091381 (J.L.H.), the Robbins Foundation (J.L.H.), Baylor Pediatrics Pilot Award (J.L.H.), Chao Physician-Scientist Award (J.L.H.), the Cytometry and Cell Sorting Core at Baylor College of Medicine with funding from the NIH (P30 AI036211, P30 CA125123, and S10 RR024574) and the expert assistance of Joel M. Sederstrom.

REFERENCE

1. Wilson HL, Wong ACC, Shaw SR, Tse W-Y, Stapleton GA, Phelan MC et al. Molecular characterisation of the 22q13 deletion syndrome supports the role of haploinsufficiency of SHANK3/PROSAP2 in the major neurological symptoms. J Med Genet 2003; 40: 575–584. [PubMed: 12920066]
2. Bonaglia MC, Giorda R, Borgatti R, Felisari G, Gagliardi C, Selicorni A et al. Disruption of the ProSAP2 Gene in a t(12;22)(q24.1;q13.3) Is Associated with the 22q13.3 Deletion Syndrome. Am J Hum Genet 2001; 69: 261–268. [PubMed: 11431708]
3. Durand CM, Betancur C, Boeckers TM, Bockmann J, Chaste P, Fauchereau F et al. Mutations in the gene encoding the synaptic scaffolding protein SHANK3 are associated with autism spectrum disorders. Nat Genet 2007; 39: 25–27. [PubMed: 17173049]
4. Moessner R, Marshall CR, Sutcliffe JS, Skaug J, Pinto D, Vincent J et al. Contribution of SHANK3 mutations to autism spectrum disorder. Am J Hum Genet 2007; 81: 1289–97. [PubMed: 17999366]
5. Leblond CS, Nava C, Polge A, Gauthier J, Huguet G, Lumbroso S et al. Meta-analysis of SHANK Mutations in Autism Spectrum Disorders: A Gradient of Severity in Cognitive Impairments. PLoS Genet 2014; 10: e1004580. [PubMed: 25188300]

6. Han K, Holder JL Jr, Schaaf CP, Lu H-C, Chen H, Kang H et al. SHANK3 overexpression causes manic-like behaviour with unique pharmacogenetic properties. Nature 2013; 503: 72–77. [PubMed: 24153177]
7. Zhu L, Wang X, Li X-L, Towers A, Cao X, Wang P et al. Epigenetic dysregulation of SHANK3 in brain tissues from individuals with autism spectrum disorders. Hum Mol Genet 2014; 23: 1563–1578. [PubMed: 24186872]
8. Yi F, Danko T, Botelho SC, Patzke C, Pak C, Wernig M et al. Autism-associated SHANK3 haploinsufficiency causes Ih channelopathy in human neurons. Science 2016; 352: aaf2669. [PubMed: 26966193]
9. Bidinosti M, Botta P, Kruttner S, Proenca CC, Stoehr N, Bernhard M et al. CLK2 inhibition ameliorates autistic features associated with SHANK3 deficiency. Science 2016; 351: 1199–203. [PubMed: 26847545]
10. Duffney LJ, Wei J, Cheng J, Liu W, Smith KR, Kittler JT et al. Shank3 deficiency induces NMDA receptor hypofunction via an actin-dependent mechanism. J Neurosci 2013; 33: 15767–78. [PubMed: 24089484]
11. Verpelli C, Dvoretskova E, Vicidomini C, Rossi F, Chiappalone M, Schoen M et al. Importance of Shank3 protein in regulating metabotropic glutamate receptor 5 (mGluR5) expression and signaling at synapses. J Biol Chem 2011; 286: 34839–50. [PubMed: 21795692]
12. Shcheglovitov A, Shcheglovitova O, Yazawa M, Portmann T, Shu R, Sebastiano V et al. SHANK3 and IGF1 restore synaptic deficits in neurons from 22q13 deletion syndrome patients. Nature 2013; 503: 267–71. [PubMed: 24132240]
13. Mei Y, Monteiro P, Zhou Y, Kim J-A, Gao X, Fu Z et al. Adult restoration of Shank3 expression rescues selective autistic-like phenotypes. Nature 2016; 530: 481–484. [PubMed: 26886798]
14. Choi S-Y, Pang K, Kim JY, Ryu JR, Kang H, Liu Z et al. Post-transcriptional regulation of SHANK3 expression by microRNAs related to multiple neuropsychiatric disorders. Mol Brain 2015; 8: 74. [PubMed: 26572867]
15. Rousseaux MWC, de Haro M, Lasagna-Reeves CA, de Maio A, Park J, Jafar-Nejad P et al. TRIM28 regulates the nuclear accumulation and toxicity of both alpha-synuclein and tau. Elife 2016; 5: 1–24.
16. Park J, Al-Ramahi I, Tan Q, Mollema N, Diaz-Garcia JR, Gallego-Flores T et al. RAS–MAPK–MSK1 pathway modulates ataxin 1 protein levels and toxicity in SCA1. Nature 2013; 498: 325–331. [PubMed: 23719381]
17. Benjamini Y, Hochberg Y. Controlling the False Discovery Rate : A Practical and Powerful Approach to Multiple Testing. J R Stat Soc 1995; 57: 289–300.
18. Gennarino VA, Singh RK, White JJ, De Maio A, Han K, Kim JY et al. Pumilio1 haploinsufficiency leads to SCA1-like neurodegeneration by increasing wild-type Ataxin1 levels. Cell 2015; 160: 1087–1098. [PubMed: 25768905]
19. Han K, Kim MH, Seeburg D, Seo J, Verpelli C, Han S et al. Regulated RalBP1 binding to RalA and PSD-95 controls AMPA receptor endocytosis and LTD. PLoS Biol 2009; 7: e100018.
20. Wang X, Xu Q, Bey AL, Lee Y, Jiang Y. Transcriptional and functional complexity of Shank3 provides a molecular framework to understand the phenotypic heterogeneity of SHANK3 causing autism and Shank3 mutant mice. Mol Autism 2014; 5: 30. [PubMed: 25071925]
21. Lee O-H, Kim H, He Q, Baek HJ, Yang D, Chen L- Y et al. Genome-wide YFP Fluorescence Complementation Screen Identifies New Regulators for Telomere Signaling in Human Cells. Mol Cell Proteomics 2011; 10: M110.001628.
22. MacLean B, Tomazela DM, Shulman N, Chambers M, Finney GL, Frewen B et al. Skyline: An open source document editor for creating and analyzing targeted proteomics experiments. Bioinformatics 2010; 26: 966–968. [PubMed: 20147306]
23. Lasagna-Reeves CA, de Haro M, Hao S, Park J, Rousseaux MWC, Al-Ramahi I et al. Reduction of Nuak1 Decreases Tau and Reverses Phenotypes in a Tauopathy Mouse Model. Neuron 2016; 92: 407–418. [PubMed: 27720485]
24. Lombardi LM, Zaghlula M, Sztainberg Y, Baker SA, Klisch TJ, Tang AA et al. An RNA interference screen identifies druggable regulators of MeCP2 stability. Sci Transl Med 2017; 9: eaaf7588.

25. Westbrook TF, Hu G, Ang XL, Mulligan P, Pavlova NN, Liang A et al. SCFβ-TRCP controls oncogenic transformation and neural differentiation through REST degradation. Nature 2008; 452: 370–374. [PubMed: 18354483]

26. LoRusso PM, Krishnamurthi SS, Rinehart JJ, Nabell LM, Malburg L, Chapman PB et al. Phase I pharmacokinetic and pharmacodynamic study of the oral MAPK/ERK kinase inhibitor PD-0325901 in patients with advanced cancers. Clin Cancer Res 2010; 16: 1924–1937. [PubMed: 20215549]

27. Ehlers MD. Activity level controls postsynaptic composition and signaling via the ubiquitin-proteasome system. Nat Neurosci 2003; 6: 231–42. [PubMed: 12577062]

28. Thomas GM, Rumbaugh GR, Harrar DB, Huganir RL. Ribosomal S6 kinase 2 interacts with and phosphorylates PDZ domain-containing proteins and regulates AMPA receptor transmission. Proc Natl Acad Sci U S A 2005; 102: 15006–11. [PubMed: 16217014]

29. O'Rawe JA, Wu Y, Dörfel MJ, Rope AF, Au PYB, Parboosingh JS et al. TAF1 Variants Are Associated with Dysmorphic Features, Intellectual Disability, and Neurological Manifestations. Am J Hum Genet 2015; 97: 922–932. [PubMed: 26637982]

30. Iossifov I, O'Roak BJ, Sanders SJ, Ronemus M, Krumm N, Levy D et al. The contribution of de novo coding mutations to autism spectrum disorder. Nature 2014; 515: 216–221. [PubMed: 25363768]

31. De Rubeis S, He X, Goldberg AP, Poultney CS, Samocha K, Ercument Cicek A et al. Synaptic, transcriptional and chromatin genes disrupted in autism. Nature 2014; 515: 209–215. [PubMed: 25363760]

32. Manousaridis I, Mavridou S, Goerdt S, Leverkus M, Utikal J. Cutaneous side effects of inhibitors of the RAS/RAF/MEK/ERK signalling pathway and their management. J Eur Acad Dermatology Venereol 2013; 27: 11–18.

33. Shin SM, Zhang N, Hansen J, Gerges NZ, Pak DTS, Sheng M et al. GKAP orchestrates activity-dependent postsynaptic protein remodeling and homeostatic scaling. Nat Neurosci 2012; 15: 1655–66. [PubMed: 23143515]

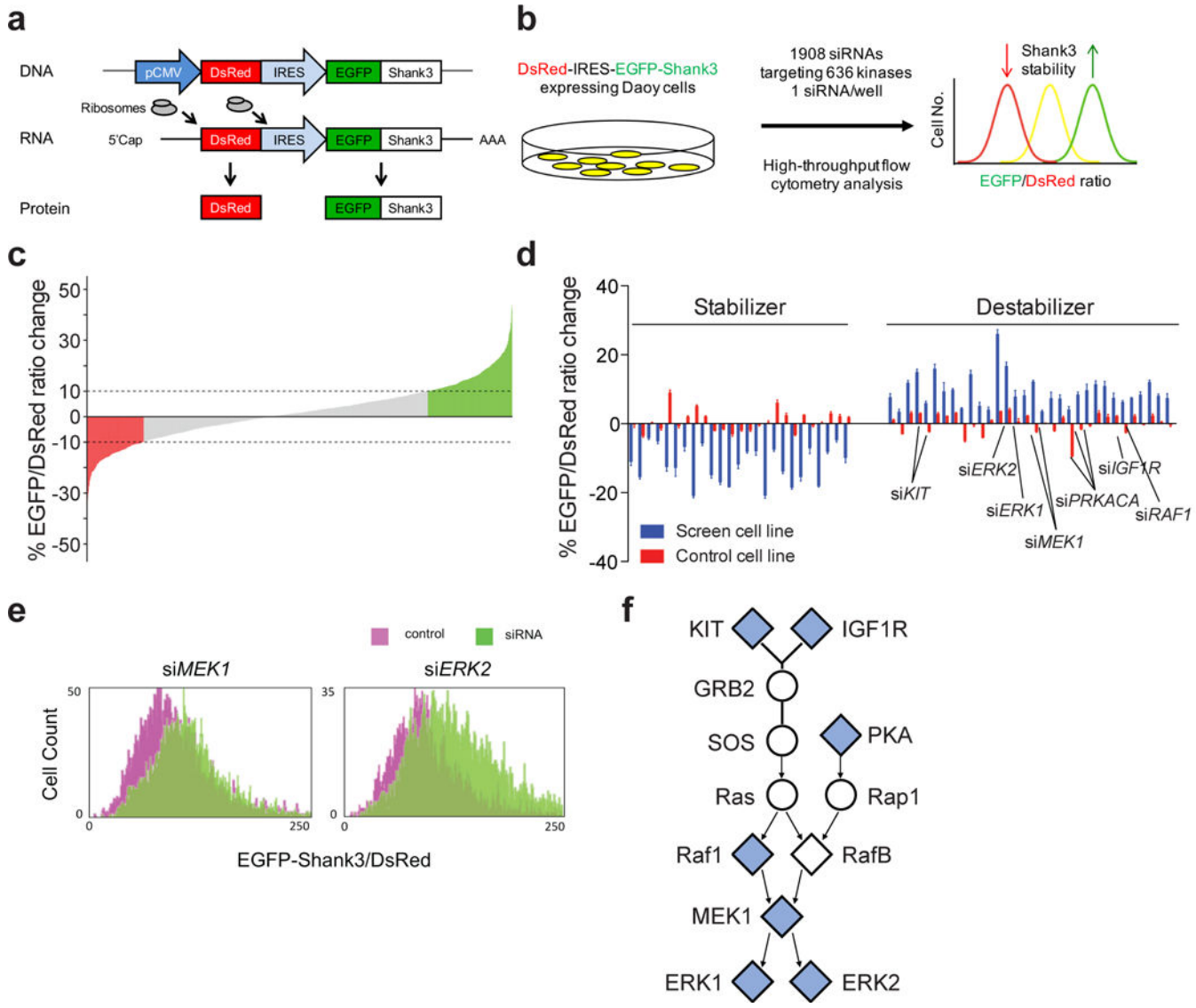

Figure 1.

A Kinome-wide RNAi screen identifies the MEK/ERK pathway regulates Shank3 stability. (**a**) Bicistronic reporter transgene allowed for monitoring of Shank3. (**b**) Schematic for the workflow of the siRNA screen against all known and putative human kinases. (**c**) Ranked percentage change of EGFP/DsRed ratio of all 1,908 siRNAs. Red bars indicate percentage changes <−10 and green bars indicate percentage changes >10. (**d**) 58 siRNA hits (representing 39 genes) from a secondary screen in which siRNAs that similarly altered the EGFP/DsRed ratio in the control cell line were eliminated. (**e**) Representative traces for EGFP/DsRed ratios upon siRNA treatment: the purple curves represent a control condition (si*Scramble*), while the green curves represent si*MEK1* and si*ERK2* mediated depletions, respectively. (**f**) Simplified MEK/ERK pathway from the KEGG database. Diamond, kinase; circle, non-kinase; blue, hits that, when knocked down, increase Shank3 stability; white, not hits or not tested. Data in **d** are presented as mean ± s.e.m..

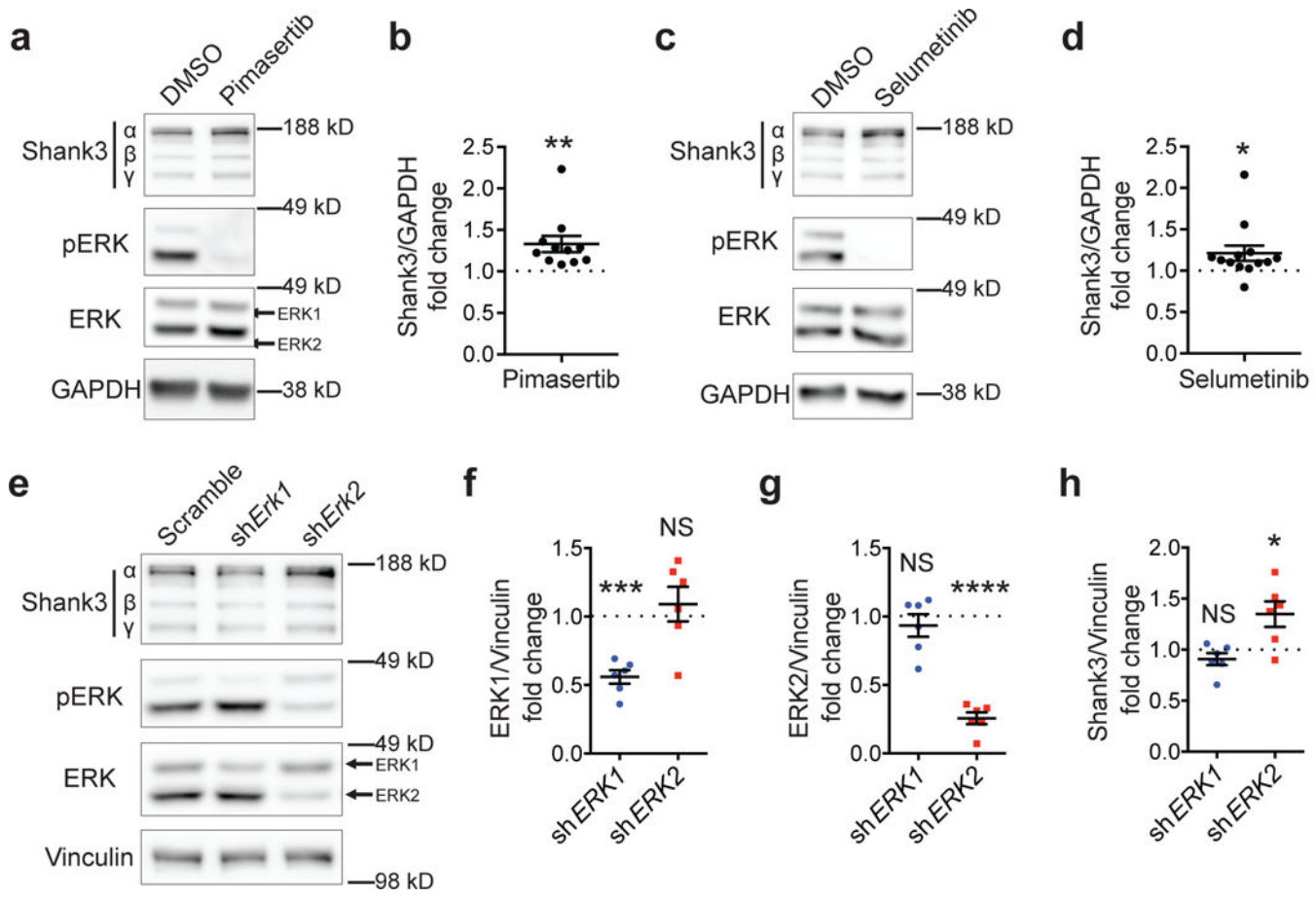

Figure 2.

Inhibition of the MEK/ERK pathway increases Shank3 abundance in neurons. (**a**) Immunoblots of Shank3, pERK, and ERK from DMSO or pimasertib (2 μM) treated primary cortical neurons. α, β, and γ indicate the three major isoforms of Shank3. GAPDH was used as loading control. (**b**) Quantification of Shank3 abundance in **a** (n=11 experiments). (**c**) Immunoblots of Shank3, pERK, and ERK from DMSO or selumetinib (0.4 μM) treated primary cortical neurons. GAPDH was used as loading control. (**d**) Quantification of Shank3 abundance in **c** (n=13 experiments). (**e**) Immunoblots of Shank3, pERK, and ERK from sh*Scramble*, sh*Erk1*, or sh*Erk2* shRNA virus-infected primary cortical neurons. Vinculin was used as loading control. (**f-h**) Quantification of ERK1 (**f**), EKR2 (**g**), and Shank3 (**h**) abundance in **e** (n=6 experiments). All data are presented as mean ± s.e.m. *p<0.05, **p<0.01, ***p<0.001, ****p<0.0001, NS, not significant; (**b**,**d**) Wilcoxon signed-rank test; (**f-h**) paired two-tailed Student's t-test.

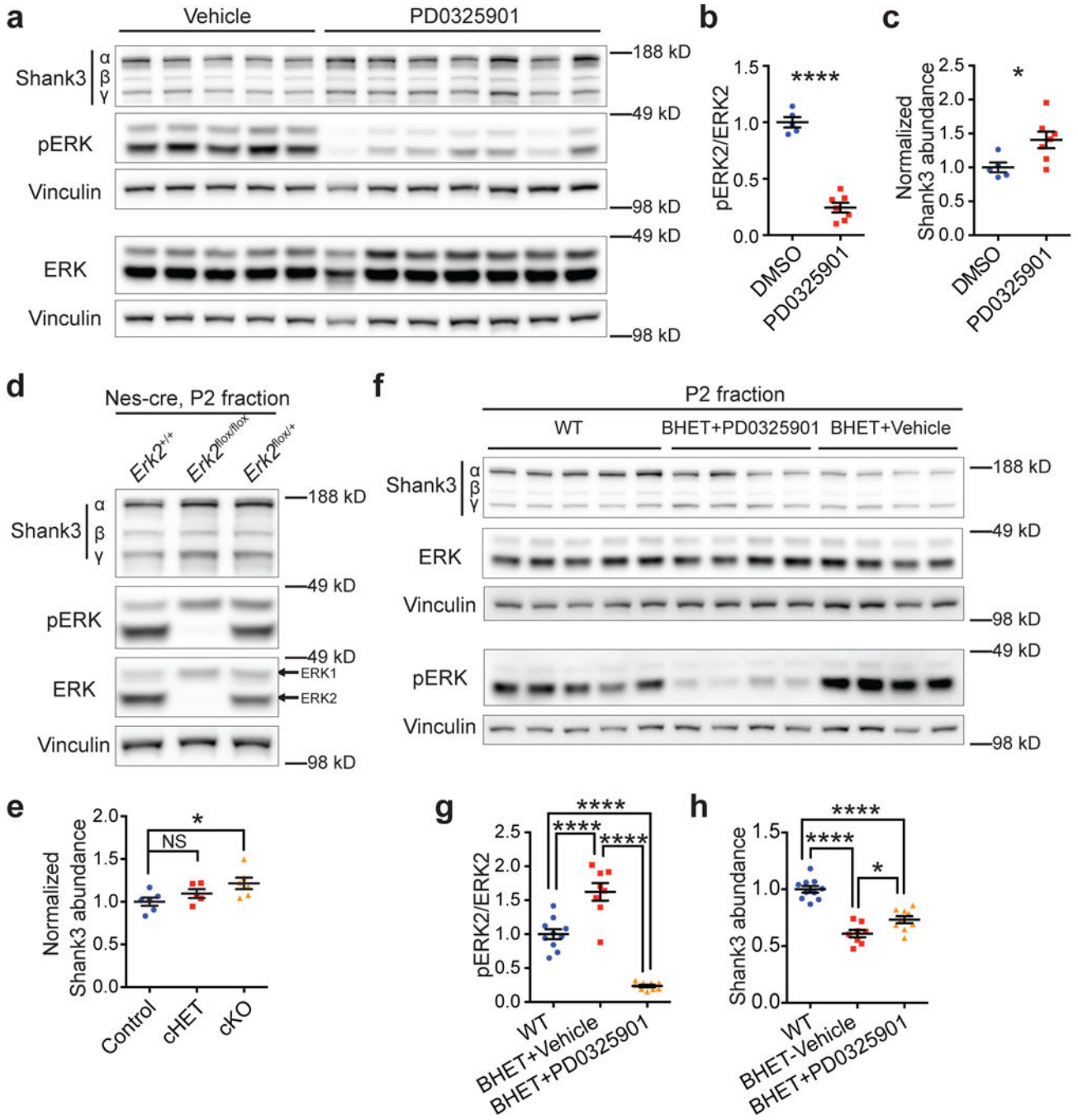

Figure 3.

Inhibition of the MEK/ERK pathway increases Shank3 abundance *in vivo*. (**a**) Immunoblots of Shank3, pERK, and ERK from the cortices of vehicle or PD0325901 injected WT mice. Vinculin was used as loading control. (**b**,**c**) Quantification of pERK/ERK (**b**) and Shank3 (**c**) abundance in **a** (n=5, 7 mice). (**d**) Immunoblots of Shank3, pERK, and ERK from the P2 fraction of cortices of control, conditional *Erk2* heterozygous, or conditional *Erk2* knockout mice. Vinculin was used as loading control. (**e**) Quantification of Shank3 abundance in **d** (n=6, 5, 6 mice). P2, crude synaptosomal fraction; cHET, conditional *Erk2* heterozygous;

cKO, conditional *Erk2* knockout. (**f**) Immunoblots of Shank3, pERK, and ERK from the P2 fraction of cortices of WT or vehicle/PD0325901 injected *Shank3B* heterozygous mice. Vinculin was used as loading control. P2, crude synaptosomal fraction; BHET, *Shank3B* heterozygous. (**g**,**h**) Quantification of pERK/ERK (**g**) and Shank3 (**h**) in **f** (n=10, 8, 9 mice). All data are presented as mean ± s.e.m. *$p<0.05$, ****$p<0.0001$, NS, not significant; (**b**,**c**) unpaired two-tailed Student's *t*-test; (**e**) one-way ANOVA with *post hoc* Dunnett's tests (multiple comparisons were carried against the control group); (**g**,**h**) one-way ANOVA with *post hoc* Tukey's tests.

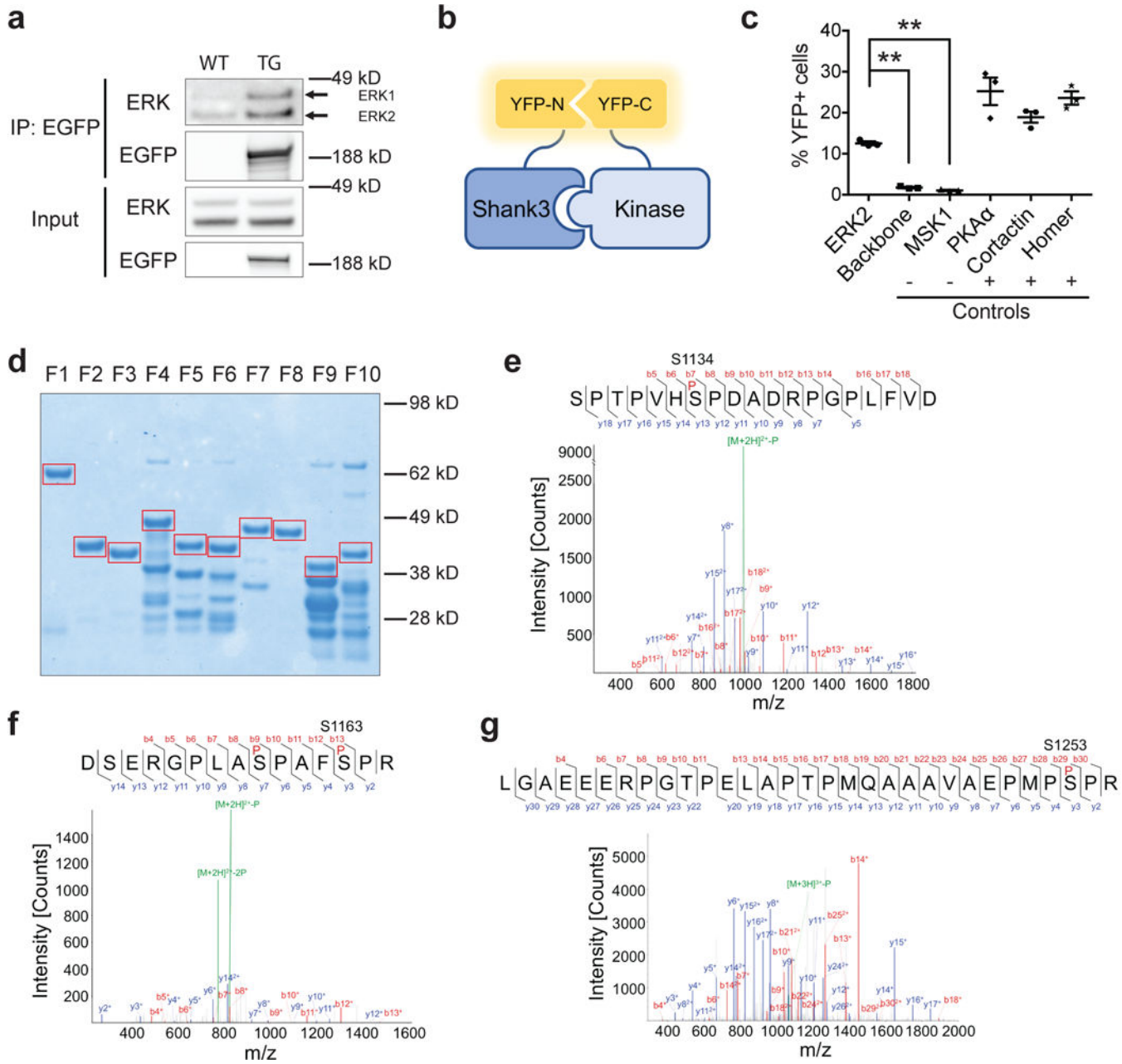

Figure 4.

ERK2 interacts and phosphorylates Shank3. (**a**) Immunoblots of ERK following immunoprecipitation of EGFP-tagged Shank3 from the *EGFP-Shank3* transgenic mice striatal lysate. TG, *EGFP-Shank3* transgenic mice. (**b**) A schematic diagram of the bimolecular fluorescence complementation assay. (**c**) Quantification of percentages of YFP positive cells of *YFP-N-Shank3* transgenic cells transfected with backbone vector or vectors expressing YFP-C tagged ERK2, MSK1, PKAα, CDK5, Cortactin, or Homer in BiFC assay (n=3 experiments). (**d**) Coomassie blue stained SDS-PAGE gel of the ten bacterially purified recombinant GST-Shank3 fragments (F1-F10) used in the kinase assay in **e**-**g**. Red rectangles indicate protein bands with predicted molecular weights of each fragment that

were excised for further mass spectrometry analysis. (**e**) Typical MS/MS spectrum of phosphorylated peptide SPTPVHpSPDADRPGPLFVD (amino acid 1128–1146 for mouse Shank3) including phosphorylated S1134 from ERK2-Shank3 *in vitro* kinase assay. (**f**) Typical MS/MS spectrum of phosphorylated peptide DSERGPLApSPAFpSPR (amino acid 1151–1165 for mouse Shank3) including phosphorylated S1163 from ERK2-Shank3 *in vitro* kinase assay. (**g**) Typical MS/MS spectrum of phosphorylated peptide LGAEEERPGTPELAPTPMQAAAVAEPMPpSPR (amino acid 1225–1255 for mouse Shank3) including phosphorylated S1253 from ERK2-Shank3 *in vitro* kinase assay. All data are presented as mean ± s.e.m. $^{**}p<0.01$; (**c**) one-way ANOVA with *post hoc* Turkey's tests.

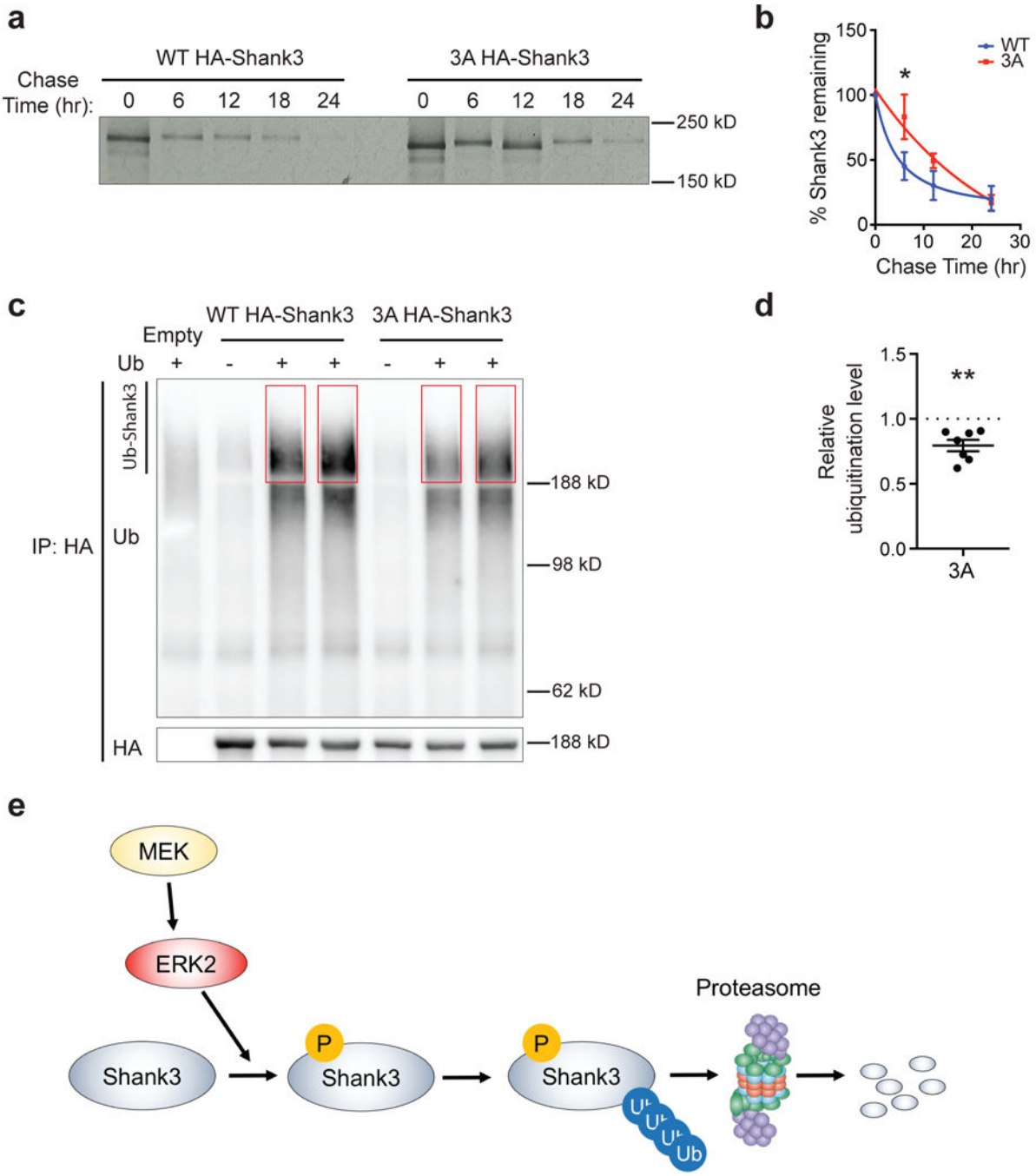

Figure 5.

Phosphorylation promotes Shank3 ubiquitination and degradation. (**a**) Autoradiography blot of immunoprecipitated HA-Shank3 from the pulse-chase assay in transfected HeLa cells. (**b**) Quantification of the HA-Shank3 signal in **a** (n=3 experiments). (**c**) Immunoblots of ubiquitin and HA following immunoprecipitation of HA-Shank3 in the ubiquitination assay. Red rectangles indicate the signals that were quantified as Ub-Shank3. Ub, ubiquitin. (**d**) Quantification ubiquitin signal in **c** (n=7 experiments). (**e**) Model for the proposed mechanism for Shank3 stability regulation by ERK2. All data are presented as mean ± s.e.m.

*p<0.05, **p<0.01; (**b**) Two-way ANOVA with *post hoc* Sidak's tests; (**d**) paired two-tailed Student's *t*-test.